INVITED PAPER *Special Section on Optical Signal-Processing Devices for Photonic Networks*

Vertically Coupled Microring Resonator Filter for Integrated Add/Drop Node

Yasuo KOKUBUN[†a)], ***Member***

SUMMARY The add/drop wavelength filter is an essential component in the new-generation photonic network. Microring resonator filters using high index contrast (HIC) optical waveguides are recently attracting attention as add/drop filters owing to their compactness, functionality such as dispersion compensation, and ease of filter synthesis. In particular, the vertically coupled microring resonator (VCMRR) filter is highly suited for the dense, large-scale integration of filter circuits. In this review, the fundamental characteristics advantageous to the add/drop filter nodes are introduced, and the recent progress in the development of vertically coupled microring resonator filters achieved mainly by the author's group is described.

key words: *microresonators, integrated optics, optical waveguide filters, high index contrast optical waveguides, add/drop wavelength filters*

1. Introduction

In the next-generation photonic network, sophisticated wavelength manipulation technologies such as wavelength add/drop, wavelength conversion, and wavelength labeling will be the key technologies. In particular, the wavelength add/drop filter is a fundamental device for extracting wavelengths to be processed from other wavelengths transmitted through the busline. Thus far, several add/drop filters, such as the acousto-optic tunable filter (AOTF) using a $LiNbO_3$ waveguide [1] and optical fiber [2], fiber Bragg grating (FBG) filter [3], waveguide grating filter [4], [5], MEMS filter [6], and microring resonator filter [7]–[10], have been proposed and demonstrated.

Among the above-mentioned filters, the microring resonator filter is suitable for the add/drop operation, because the external RF control signal which is required in AOTF's, and the circulator which is required in FBG's and Fabry-Perot MEMS filters are unnecessary, and because of the possibility of filter response synthesis. In addition, the microring resonator filter has many other advantages including compactness [9], [10] and functionality such as dispersion compensation [11], [12], nonlinear enhancement [13], and signal processing [14].

However, there have been some problems with conventional microring resonators, such as the difficulty of precise control of the coupling strength between the busline and the microring, which is essential for achieving the desired bandwidth, and the difficulty of dense integration.

To solve the above problems, we have proposed and demonstrated a vertically coupled microring resonator (VCMRR) filter as the building block of integrated photonic filter circuits [15]–[22], [26]–[28], [30], [31], [33]–[35], [37]–[39], [41]–[43], [45]. In this review, the fundamental characteristics and features of microring resonators are introduced first in Sects. 2.1 and 2.2. Next the history of the research on microring resonator filters is briefly reviewed in Sect. 2.3. In the following sections, recent progress in the development of vertically coupled micro-ring resonator filters, such as the fabrication process (Sect. 3), multilevel busline (Sect. 4), center wavelength trimming and tuning (Sects. 5 and 6), and new integration technology (Sect. 7), is summarized.

2. Fundamental Characteristics of VCMRR

2.1 Device Structure and Features

The fundamental structure of VCMRR is shown in Fig. 1. An ultracompact ring resonator can be realized by using high index contrast (Δ=34–37%) waveguide consisting of a dielectric material core (Ta_2O_5-SiO_2 compound glass with n=1.8, or SiN with n=2.0) and an air cladding, in the vertically coupled configuration [15] where a microring resonator with a radius of approximately 10 μm is stacked on the crossing point of cross-grid busline waveguides [16], as shown in Fig. 1. Due to the high index contrast, the stacked configuration and the cross-grid topology, this filter element has the following advantages.

(1) Owing to the stacked configuration, the upper and lower waveguides play different roles, i.e., the lower buried channel waveguides serve as input/output busline

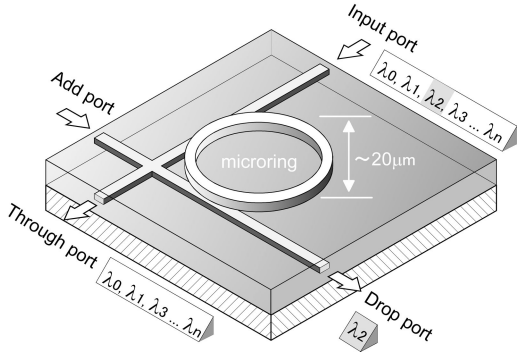

Fig. 1 Perspective view of single-channel VCMRR.

Manuscript received August 2, 2004.
Manuscript revised October 24, 2004.

[†]The author is with Graduate School of Engineering, Yokohama National University, Yokohama-shi, 240-8501 Japan.
a) E-mail: kokubun@ynu.ac.jp

DOI: 10.1093/ietele/e88–c.3.349

waveguides while the ring functions as the frequency-selective element.

(2) Owing to the high index contrast in the upper layer, an ultracompact ring resonator with a very small radius of 10 to 20 μm, which exhibits the bandwidth of 0.1 to 1.0 nm and the free spectral range (FSR) of 10 to 25 nm, is possible. This narrow bandwidth leads to the high Q (1,500–15,000) of the microring resonator filters.

(3) Owing to the ultracompact element and the cross-grid configuration, a dense integration of up to 10^4 – 10^5 devices/cm^2 is possible.

(4) The coupling strength between the ring and busline waveguides can be controlled more precisely than the lateral coupling, because vertical separation is achieved via well-controlled deposition, rather than etching of fine gaps.

(5) In vertical coupling, the fabrication tolerance of the lateral misalignment between the upper microring and lower busline waveguide is relaxed, because the overlap of the field profile is maximum at the point of zero offset, and is much less sensitive to the offset than in lateral coupling.

(6) The cross-grid topology makes it possible to adapt the same configuration to many coupled ring topologies, such as the series coupled, parallel coupled, and cascaded topologies.

2.2 Transfer Function of Ring Resonator

Let us assume a ring resonator with radius R coupled to a busline waveguide and add/drop waveguide, as shown in Fig. 2. When the propagation constants in the ring resonator and the busline and add/drop waveguides are all the same, the coupling strength of the optical field in the coupling region can be expressed by $\cos(\kappa l)$ to the through port and $j\sin(\kappa l)$ to the drop port. Thus $\sin^2(\kappa l)$ corresponds to the power fraction coupled from the busline waveguide to the ring waveguide, and $\cos^2(\kappa l)$ corresponds to that which passes straight through the busline waveguide. Then the transfer function of optical power to the drop port is expressed by

$$T(\lambda) = \frac{|Y|^2}{(1-X)^2 + 4X\sin^2\dfrac{\phi(\lambda)}{2}}, \tag{1}$$

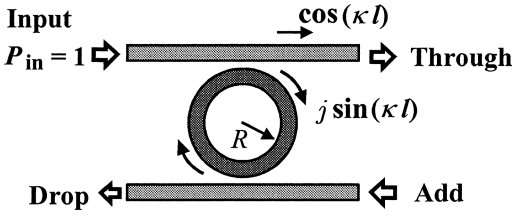

Fig. 2 Definition of coupling coefficient in a single-ring resonator. P_{in} is the input optical power (normalized to unity), R is the ring radius, κ is the coupling coefficient, and l is the equivalent coupler length.

where the parameters X, Y and $\phi(\lambda)$ are given by

$$X = \cos^2(\kappa l)\exp\left(-\frac{\alpha L}{2}\right), \tag{2}$$

$$Y = \sin^2(\kappa l)\exp\left(-\frac{\alpha L}{4}\right), \tag{3}$$

$$\phi(\lambda) = \beta L = \frac{2\pi n_{eq} L}{\lambda}. \tag{4}$$

Here, L (=$2\pi R$) is the path length in the ring, n_{eq} is the equivalent refractive index in the ring and busline waveguides (= β/k_0, k_0 is the propagation constant in a vacuum), and α is the propagation loss coefficient.

The theoretical drop port response calculated by Eqs. (1)–(4) is shown in Fig. 3. The response shape is expressed by the Airy function, and is sometimes approximated by the Lorentzian function. In this calculation, the propagation loss in the ring waveguide was assumed to be zero (α=0), and the parameter is the product of the coupling coefficient and equivalent coupler length. The peak wavelength is given by the wavelength satisfying $\phi(\lambda)$=$2m\pi$, where m is the resonance order, and is expressed by

$$\lambda_m = \frac{n_{eq} L}{m}. \tag{5}$$

On the other hand, the spacing between peak wavelengths, which is called the free spectrum range (FSR), is given by

$$FSR = \Delta\lambda = -\frac{\lambda^2}{2n_{eff}\pi R}, \tag{6}$$

where n_{eff} is the effective equivalent index defined by

$$n_{eff} = n_{eq}\left(1 - \frac{\lambda}{n_{eq}}\cdot\frac{dn_{eq}}{d\lambda}\right). \tag{7}$$

It is seen from Fig. 4 that the bandwidth (full width at half maximum, FWHM) of the pass band and the rejection (crosstalk) in the rejection band depend on the coupling strength between the busline waveguide and the ring resonator. In other words, the finess is defined by the ratio of

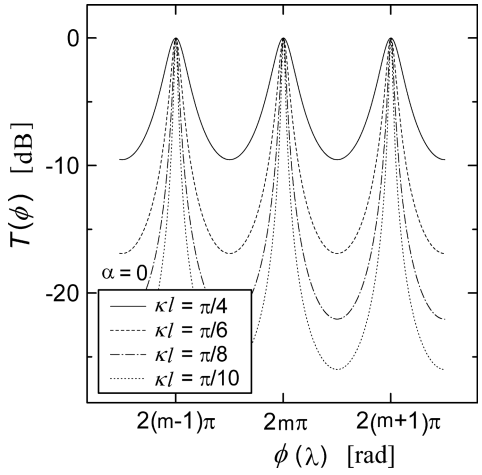

Fig. 3 Theoretical dropping response of single-ring resonator.

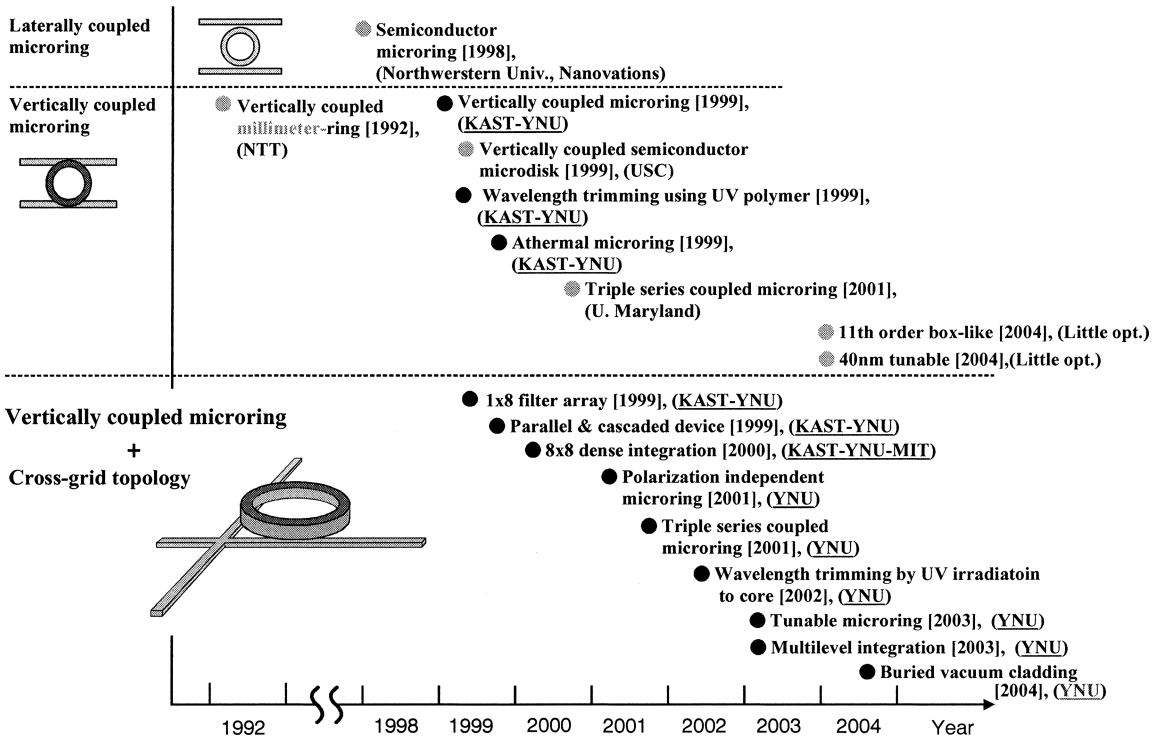

Fig. 4 History of research on microring resonator filter.

FSR to bandwidth (FWHM).

As an example, let us design the FSR to be 20 nm and the bandwidth to be 0.4 nm at the wavelength of 1550 nm, which corresponds to the finess of 50. From Eq. (6), the product $n_{eq}R$ is calculated to be 19.12 μm. When the effective equivalent index is 1.7 using a high index contrast waveguide, the required ring radius is 11.2 μm. Therefore, to achieve a wide FSR greater than 10 nm, a small ring radius of less than 20 μm is required. On the other hand, the coupling strength required to achieve the finess of 50 is 6% ($\sin^2(\kappa l) = 0.06$). In the VCMRR, the propagation constants in the busline waveguide and the microring are not exactly equal to each other. Consequently the coupling strength cannot reach 100%. However, although the coupling is a kind of asymmetric coupling, a coupling strength ranging from 5% to 15% can be easily obtained by controlling the thickness of the buffer layer, and hence the achievable finess is greater than 50.

2.3 History of Research on Microring Resonator Filter

Since the first proposal of the optical waveguide ring resonator [23], the waveguide ring resonator has been utilized as the cavity of a ring laser and in some sensor applications [24]. However, the ring radius was of the order of millimeters, and so the FSR was too small to be used as the wavelength filter for dense WDM systems. In 1997, a group from MIT proposed the microring resonator for an add/drop filter, the ring radius of which was of the order of 10–50 μm [7]. To realize this tiny ring radius, a high index contrast waveguide with an index difference greater than 20% was needed. From late 1997 to 1999, a microring resonator filter was demonstrated using a semiconductor waveguide with an air cladding [8]–[10], [25]. However, since the structure of this device was planar, where the ring and the busline waveguides were formed in the same layer, a very precise fabrication technique was needed to form a very fine gap between the busline and the microring.

On the other hand, to solve this problem, we proposed and demonstrated the vertically coupled microring resonator [15] in 1999. Aslo in the same year, we demonstrated the vertically coupled microring resonator with a cross-grid busline topology [16]. After these first demonstrations, we developed the design and fabrication technologies for the improvement of the fundamental characteristics and for the dense integration of filter circuits. The history of research on the microring resonator filter is summarized in Fig. 4.

2.4 Filter Synthesis by Coupled and Cascaded Topologies

For the wavelength filters used in the DWDM system, the following requirements must be satisfied: (a) the bandwidth of the pass band must be wide enough to cover the signal spectrum (typically 50–80 GHz), (b) the pass band spectrum response should have a flat top to prevent the deformation and loss of the signal spectrum, (c) the transition from the pass band to the rejection band should be narrow, i.e., the roll-off should be sharp, (d) the crosstalk in the rejection band must be sufficiently small, (e) the spectrum response must be temperature independent and polarization indepen-

dent, and (f) the dispersion in the pass band must be sufficiently small.

However, it is difficult for a single microring resonator to satisfy all these requirements because the spectral response expressed by the Lorentzian function has a sharp peak and involves a large winglike crosstalk in the rejection band. Thus a filter response synthesis is needed. Fortunately, the filter response of the ring resonator can be synthesized by the combination of coupled and cascaded topologies. In addition, since the VCMRR is advantageous for dense integration due to its very compact element and cross-grid topology, it is easy to form the coupled and cascaded topologies without deteriorating the compactness.

There are three basic topologies in the combinations of ring resonators, i.e., series coupling, parallel coupling, and cascaded topology, as shown in Fig. 5. The advantages and drawbacks of these topologies are summarized in Table 1.

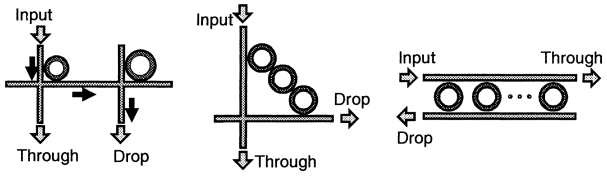

(a) Cascading. (b) Series coupling. (c) Parallel coupling.

Fig. 5 Basic topologies of combinations of ring resonators.

Table 1 Topologies of ring filter circuit.

Topology	Advantages	Drawbacks
Cascading	Expansion of FSR Reduction of crosstalk	Loss increase due to center wavelength mismatch
Series coupling	Expansion of FSR Flat-top pass band	Small fabrication tolerance
Parallel coupling	Flat-top pass band	Small fabrication tolerance

3. Fabrication Technology of VCMRR

3.1 Conventional Fabrication Process

Figure 6 shows the fabrication process of a single VCMRR. In the early stage of our study, the waveguide core layers were made of Ta_2O_5/SiO_2 compound glass (Ta_2O_5 30 mol%, n=1.785 @ λ=1550 nm), and the cladding and separation layers were SiO_2 (n=1.451 @ λ=1550 nm). All the layers were deposited by an RF sputtering technique and the core was patterned by photolithography and reactive ion etching (RIE). Two years ago, we introduced a plasma enhanced chemical vapor deposition (PECVD) apparatus, and SiN (n=2.04 @ λ=1550 nm) and SiON (n=1.65–1.85 @ λ=1550 nm) were used as the core material. The cladding of the microring resonator is air, and so the index contrast is 34% for the Ta_2O_5/SiO_2 core and 37% for the SiN core.

The key point of this fabrication process is some technologies which were newly developed to obtain a flat-top surface of the busline waveguide. To achieve this, we developed the lift-off process shown in Fig. 6. In this lift-off process, first, the lower busline waveguide core is formed by RIE using the Cr mask, and the ridge-shaped core is buried by SiO_2 using a bias-sputtering deposition technique. The SiO_2 layer on the core is eliminated by the lift-off process

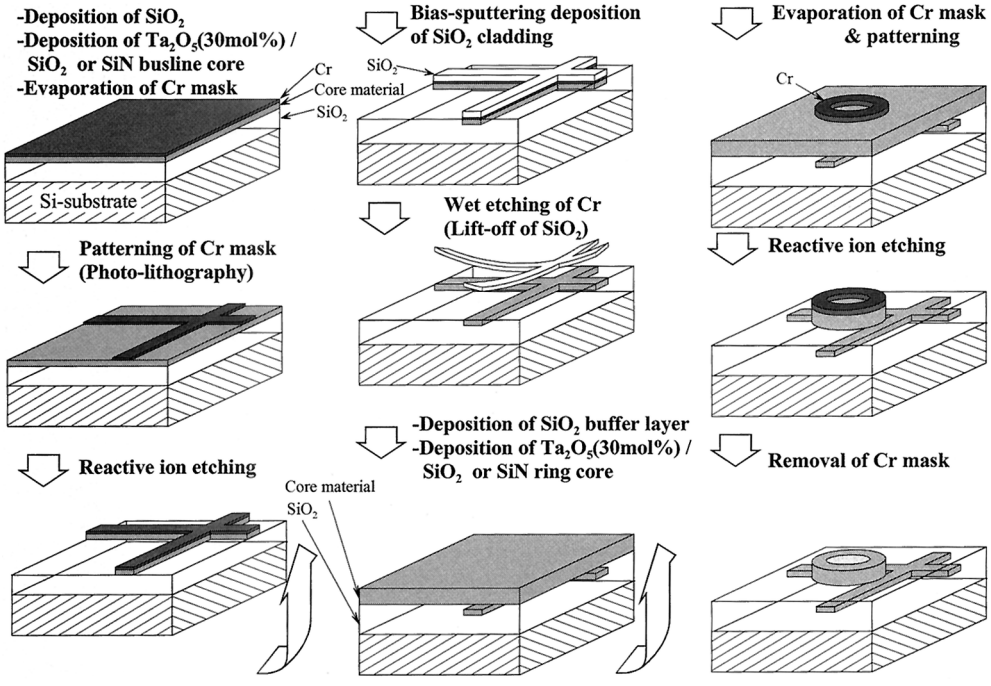

Fig. 6 Fabrication process of VCMRR.

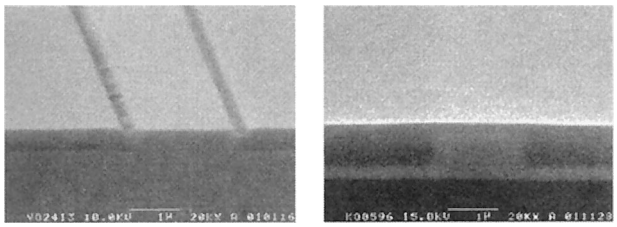

(a) Fabricated by conventional lift-off process. (b) Fabricated by improved process using SOG.

Fig. 7 SEM bird's-eye-view images of cross section of busline waveguide.

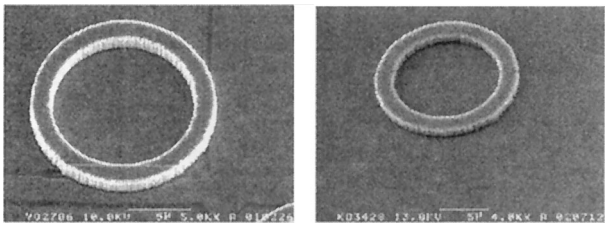

(a) Fabricated by conventional lift-off process. (b) Fabricated by improved process using SOG.

Fig. 8 SEM bird's-eye-view images of vertically coupled microring resonator with air cladding.

using wet chemical etching of the Cr mask. Due to this lift-off process, the bump height of the top of the busline waveguide can be reduced to be less than 0.1 μm, as shown in Fig. 7(a).

3.2 Improved Fabrication Process for Planarization

The small step height should be perfectly planarized to reduce the scattering loss in the ring resonator. In particular, a perfectly planarized top surface is needed to enable the multilevel stacking of the waveguides. Thus we developed an improved fabrication process using a spin-on-glass (SOG) to planarize the top surface of the buried waveguide [26]. SOG is a liquid material before baking, and its thin film (about 0.2 μm) can be formed by spin-coating and baking. Due to the characteristic of spin-coating, a small step height of less than 0.1 μm can be perfectly planarized, as shown in Fig. 7(b). After spin-coating, the film is baked in nitrogen atmosphere at the temperature of 400°C for 40 minutes and an additional buffer layer is deposited.

The SEM cross-sectional images of busline waveguides formed by the conventional process and the improved process using SOG are shown in Figs. 7(a) and (b). The SEM images of microrings fabricated on busline waveguides buried by the conventional and the new process are shown in Figs. 8(a) and (b).

3.3 Fine Fabrication Process of Smooth Side Wall

Another key issue of the fabrication process is the vertical and smooth side wall of the microring resonator. This is very important for reducing the scattering loss of the ring

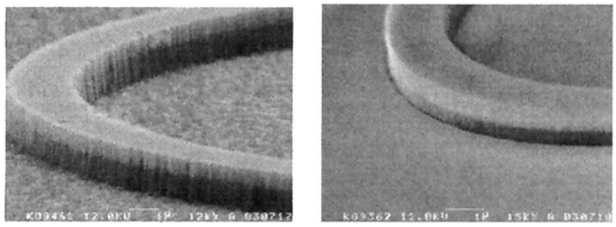

(a) Fabricated by conventional wet etching of Cr mask. (b) Fabricated by improved dry etching of Cr mask.

Fig. 9 SEM bird's-eye-view images of microring fabricated using a Cr mask formed by wet chemical etching and RIE.

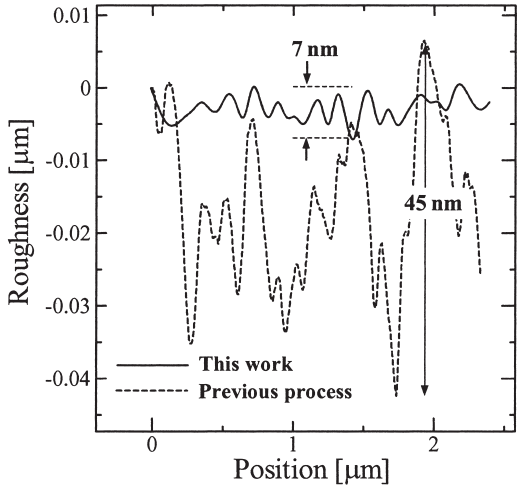

Fig. 10 Surface roughnesses of side wall fabricated by the conventional fabrication process and the fine fabrication process of a smooth side wall.

waveguide. Because the index contrast of the ring waveguide is extremely high ($\Delta > 30\%$) and the ring radius is very small (~10 μm), the field profile of the guided mode in the microring is localized around the outer side wall of the microring. Therefore, the scattering loss is easily increased by the roughness of the side wall.

However, it is seen in Fig. 8(b) that some appreciable amount of roughness remains on the side wall of the microring waveguide. By carefull observation of the side wall after each fabrication process, it was found that this roughness appears after the patterning of the Cr mask by wet chemical etching. Thus we changed the patterning process of the Cr mask from wet chemical etching to reactive ion etching (RIE) using O_2 gas and a silicone-based positive photoresist. As a result, the roughness of the side wall was greatly reduced from 45 nm to 7 nm, as shown in Figs. 9(a) and (b).

Figure 10 shows the side wall roughnesses of waveguides with Cr masks fabricated by conventional wet chemical etching and by RIE. The roughness of the side wall shown in Fig. 10 was measured by preparing some straight waveguide patterns with the direction slightly at angle to the crystal orientation of the Si substrate. A cross section of the Si substrate was prepared by cleaving, so that the side wall of the waveguide appears on some part of the cleaved surface. The roughness was measured using a scanning elec-

tron microscope (SEM) equipped with a surface roughness measurement option.

4. Fabrication of VCMRR with Multilevel-Crossing Busline Waveguide and Ultracompact Ring Radius

4.1 Ultracompact Ring Radius and Wide FSR

Using the fabrication process described in Sect. 3.3, we fabricated the microring resonator shown in Fig. 1, which has a ring radius of 5 μm. The core material of microring and busline waveguides is Ta_2O_5/SiO_2 compound glass (Ta_2O_5 30 mol%, n=1.785 @ λ=1550 nm), and the cladding and separation layers are SiO_2 (n=1.451 @ λ=1550 nm). The width and thickness of the ring core are 1.2 μm and 0.7 μm, respectively. The thickness of the separation layer between microring and busline waveguides is 0.6 μm. The filter response was measured using a tunable laser and an optical spectrum analyzer.

The measured drop port response is shown in Fig. 11. An extremely wide free spectrum range (FSR) of 37 nm was obtained. To our knowledge, this FSR is the widest value for a single ring resonator reported so far. If a semiconductor waveguide is used as the ring core [8]–[10], the optical path length in a resonator with the same 5 μm radius is much longer than that of the microring made of dielectric material with an index of around 2.0, and the FSR is limited to about 20 nm.

To compare the filtering characteristics, we fabricated the microring resonators shown in Fig. 1, which have a ring radius of 20 μm, by the conventional process as well as with the fine fabrication process for a smooth side wall. The materials and the dimensions are the same as those of the device with the ring radius of 5 μm, except for the ring radius. The measured filter responses from the drop port and through port are shown in Figs. 12(a) and (b), respectively. The −3 dB bandwidth of the drop port response was improved from 0.3 nm to 0.2 nm, and the rejection depth of the through port response was greatly improved from −4 dB to −19 dB. Using these measured data, the propagation loss in the microring was evaluated employing the simultaneous equation [27]. The propagation loss was greatly improved from 0.47 dB/turn to 0.066 dB/turn.

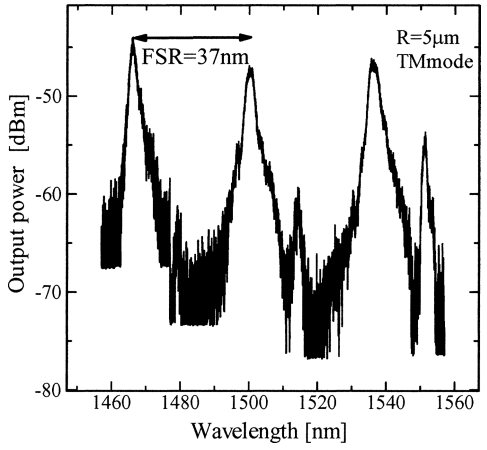

Fig. 11 Measured drop port response of VCMRR with the ring radius of 5 μm fabricated by the fine fabrication process of a smooth side wall.

4.2 VCMRR with Multilevel-Crossing Busline Waveguide

Using the new fabrication process for planarization described in Sect. 3.2, a single ring resonator with a multilevel-crossing busline waveguide [26], as shown in Fig. 13, was fabricated. The core and cladding materials were the same as those described in the preceding subsection. The width and thickness of the ring core were 1.5 μm and 1.0 μm, respectively. The thickness of the separation layer was 0.5 μm, and the ring radius was 25 μm. Since the microring core was buried by the SiO_2 cladding, the core width of 1.5 μm satisfies the single mode condition.

The filter response was measured using a tunable laser and an optical spectrum analyzer. The measured responses at the through port and the drop port are shown in Fig. 14. Clear filter responses with the FSR of 8.4 nm and the FWHM bandwidth of 0.49 nm were observed [26]. The insertion loss of this device is larger than 15 dB, because the spot-size of the busline waveguide (1.5–2.0 μm) is much smaller than that of the single mode fiber. This will be improved by introducing a spot-size transformer [28].

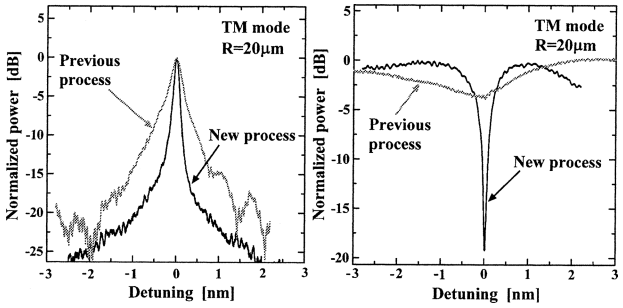

(a) Drop port responses. (b) Through port responses.

Fig. 12 Comparison of filter responses of VCMRR fabricated by the conventional fabrication process and the fine fabrication process of a smooth side wall.

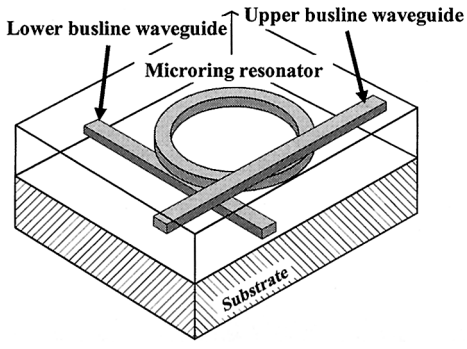

Fig. 13 Vertically coupled microring resonator filter with multilevel-crossing busline waveguide.

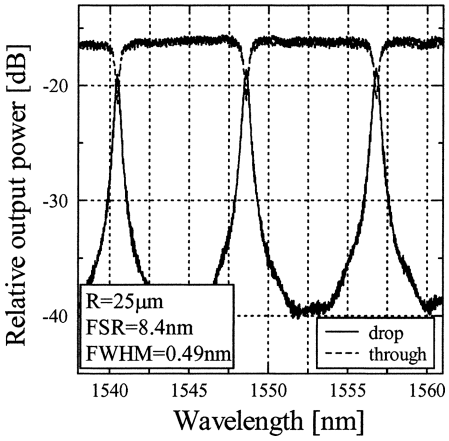

Fig. 14 Measured filter response of single microring resonator filter with multilevel-crossing busline waveguide (TE mode).

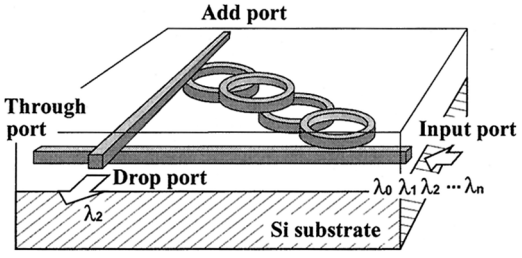

Fig. 15 Quadruple series coupled microring resonator filter with multilevel-crossing busline waveguide.

A vertical quadruple series coupled microring resonator with multilevel-crossing busline waveguides, as shown in Fig. 15, was also fabricated by the same fabrication process. In contrast to the single-ring device shown in Fig. 13, this structure consists of two core layers, i.e., both layers involve the busline waveguide and the microring resonator and those waveguides are coupled to each other in the vertical direction. Therefore, all the couplings between the busline and microrings and between the microrings themselves can be precisely controlled by controlling the vertical distance, i.e., the thickness of the separation layer. In addition, the busline waveguides are also crossed in different layers, so that scattering will not occur at the crossing point.

The measured filter response of the quadruple series coupled microring resonator with the ring radius of 60 μm is shown in Fig. 16. A clear filter response with the FWHM bandwidth of 1.12 nm and the FSR of 3.5 nm was observed. In addition, due to the quadruple series coupled configuration, a boxlike filter response [29]–[32] was obtained. A small ripple of about 1.5 dB was observed in the pass band. This seems to be caused by the strong coupling between microrings as well as by the small difference in the resonant wavelengths between four microrings, which is due to fabrication error and can be reduced by improving the fabrication accuracy. The shape factor, which is defined by the ratio of the -1 dB bandwidth to the -10 dB bandwidth, was evaluated to be 0.66, which is close to the theoretical value of

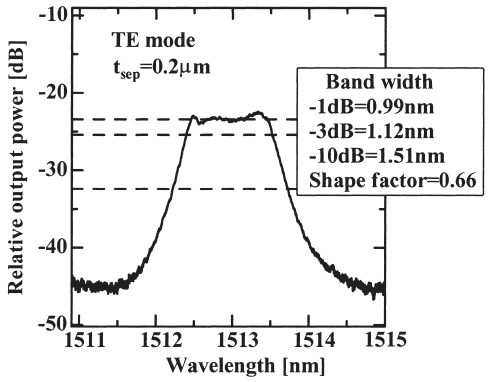

Fig. 16 Measured filter response of quadruple series coupled microring resonator filter with multilevel-crossing busline waveguide.

0.68 for the quadruple series coupled ring resonator with a maximally flat condition.

Recently, the very high order of an eleven series coupled microring was reported and a very square dropping response with very low insertion loss was obtained [32], which is not easy to accomplish in the flat-top AWG.

5. Center Wavelength Trimming by UV Irradiation

In our previous work, we demonstrated 1×8 channel dropping filter array [16]. However, the accuracy of the center wavelength was not high enough for DWDM systems, as shown in Fig. 17 [33]. In Fig. 17, the center wavelegth of 1×8 VCMRR filter arrays made of SiN and Ta_2O_5-SiO_2 compound glass (Ta_2O_5 30 mol%) are plotted against the ring radius. The ring radii of the array increased from 10.00 μm of the first one to 10.35 μm of the last one with increments of 50 nm, which corresponds to the channel spacing of 5.7 nm. It is seen from this figure that the maximum error of the center wavelength was 3.7 nm for the microring with the SiN core. This error seems to be due to the fabrication error in the photolithography process. Thus, a trimming technique with a trimming range greater than 4 nm is required to compensate for the fabrication error.

To develop a trimming technique, we measured the UV-induced refractive index change of SiN film deposited by a plasma-enhanced CVD method using SiH_4. The refractive index was measured using a prism coupler (Metricon PC-2010). An Ar ion SHG laser (λ=244 nm, spot size =0.35 mm) was used as the UV light source, and the power was 100 mW. From this measurement, we discovered that the maximum UV-induced index change of SiN is as large as -1.30×10^{-2}, as shown in Fig. 18. Owing to this large index change, a wide trimming range of the center wavelength of up to -11.4 nm can be expected. In addition, the change of the SiN refractive index was stable for more than 1000 hours without the hydrogen loading that was required for the UV index change of Ta_2O_5-SiO_2 compound glass [33] and Ge-doped silica glass.

Utilizing the large UV-induced refractive index change of SiN, we demonstrated wide-range trimming of the cen-

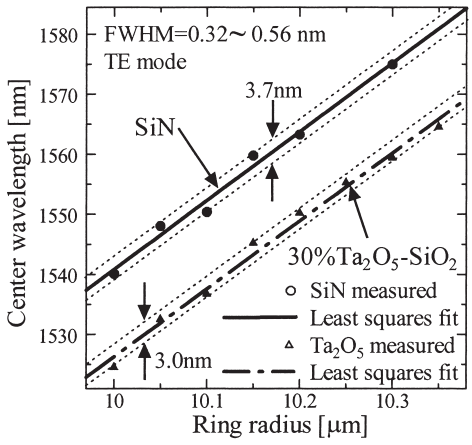

Fig. 17 Center wavelength vs ring radius of 1 × 8 microring filter arrays made of SiN and Ta_2O_5-SiO_2.

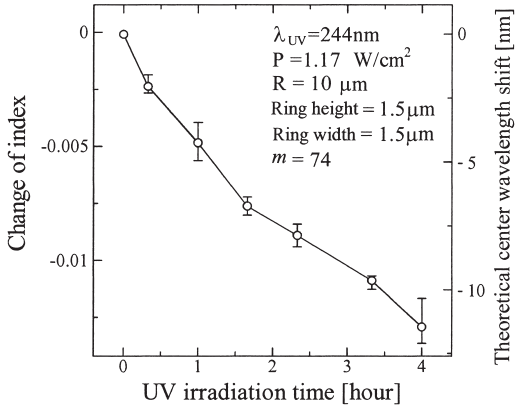

Fig. 18 UV-induced refractive index change of SiN film and theoretical center wavelength shift against UV irradiation time.

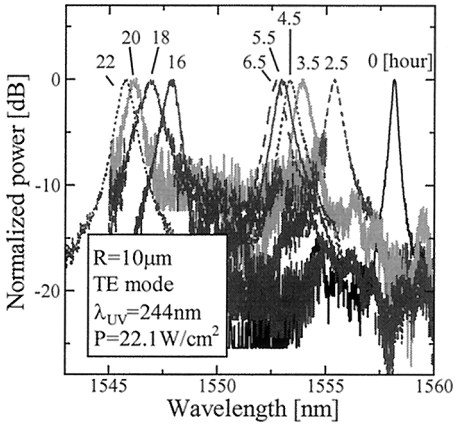

Fig. 19 Change of filter response of VCMRR against UV irradiation time.

ter wavelength of the VCMRR. One resonator in the 1×8 filter array was exposed to the UV laser beam for several hours up to 22 hours, and the filter response was measured at each accumulated irradiation time. The results are shown in Fig. 19. A wide trimming range of −12.1 nm was successfully demonstrated [34], [35]. This value coincides with

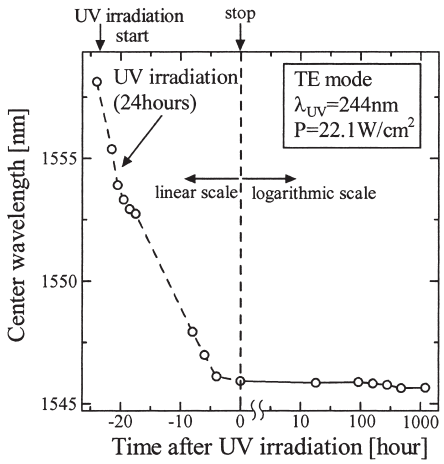

Fig. 20 Change of center wavelength of VCMRR against time.

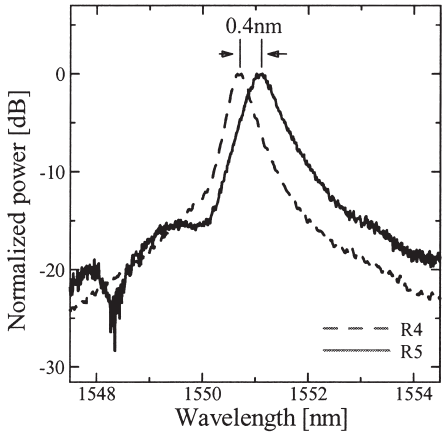

Fig. 21 Demonstration of narrow channel spacing by shifting the center wavelength of ring #5 to that of ring #4.

the theoretical value of −11.4 nm calculated from the UV-induced index change.

Lastly, the stability of UV trimming was measured for 1200 hours. The result is shown in Fig. 20. It was confirmed that SiN deposited by plasma-enhanced CVD using SiH_4 has a high UV sensitivity and long-term stability, and is suitable for the center wavelength trimming of the VCMRR filter [34].

Using this UV trimming technique, precise control of the wavelength channel spacing was demonstrated [35]. The center wavelengths of rings #4 and #5 in the filter array were separated by 7.6 nm. For each step-by-step irradiation of the UV laser beam (spot size of 0.35 mm) on only ring #5, the center wavelength was measured. As a result, the center wavelength of ring #5 was shifted closer to that of ring #4, and a small channel spacing of 0.4 nm was successfully obtained, as shown in Fig. 21.

6. Tunable VCMRR Using TO Effect of Polymer Core

A wide-range tunable add/drop filter is demanded for the flexible and scalable photonic network. However, a wide-

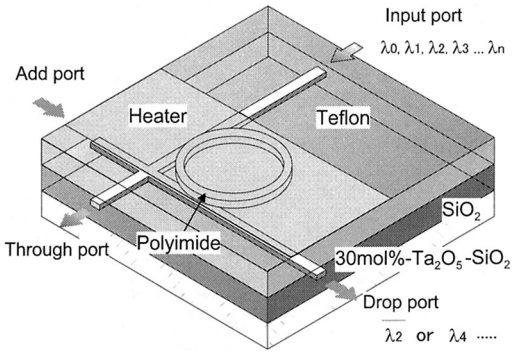

Fig. 22 Tunable microring resonator filter made with polymer core and integrated microheater.

range tunable microring resonator filter has not been reported due to the difficulty of changing the refractive index of the core material over a wide range [36]. Thus we adopted a polymer as the core material of the VCMRR, because the temperature dependence of the refractive index (TO coefficient) of polymer materials is generally much stronger than that of glass materials by more than one order of magnitude.

Figure 22 shows the structure of the tunable microring resonator filter with an integrated microheater [37], [38]. The microring core is made of polyimide (n=1.74 @ λ=1.55 μm) and the upper cladding of the microring is Teflon (n=1.30 @ λ=1.55 μm). The microring core and upper cladding polymer layers were formed by spin-coating. This ultrahigh index contrast (Δ=22%) enables a small ring radius of 10 μm, and the flat top surface of the over-cladding layer resulting from the spin-coating of Teflon enables the integration of microheater on top of the microring. In addition, the high glass-transition temperature of polyimide and Teflon enables a wide range of tuning simply by heating the device to high temperatures.

In contrast to this, the busline waveguide was made of a Ta_2O_5-SiO_2 core (n=1.79) and SiO_2 cladding (n=1.45). The busline waveguide layers were formed by RF sputtering.

An integrated microheater made of aluminum was installed to control the surface temperature with low power consumption.

First, the temperature dependence of the center wavelength of the VCMRR filter without the microheater was measured using an external heater. The results are shown in Fig. 23. The center wavelength was shifted by 18 nm with the temperature increase of 150°C. This temperature is almost the same as the glass-transition temperature of Teflon (that of polyimide is about 300°C). From the result of this experiment, the temperature coefficient of the center wavelength was evaluated to be −0.14 nm/°C, which is almost ten times greater than that of silica-based waveguide filters [36].

The reproducibility of the filter response was confirmed by the heat cycle test. The change of the center wavelength was less than 0.1 nm, as shown in Fig. 24 [37].

Next, another tunable VCMRR with an integrated microheater was fabricated and the change of the center wavelength was measured by changing the electric current supplied to the heater. The result is shown in Fig. 25. A wide range of tuning of 9.4 nm was successfully demonstrated [37]. The FWHM bandwidth of the filter response was not changed during this tuning. This result implies that the poly-

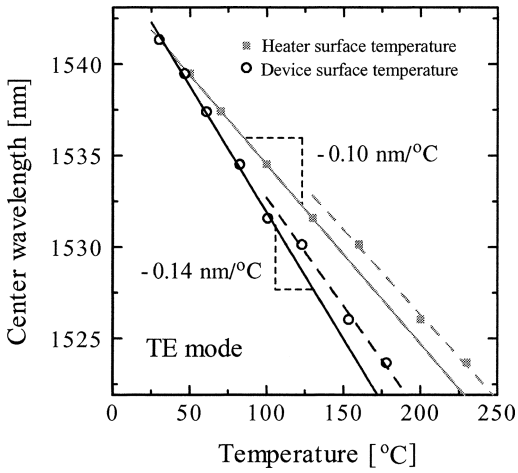

Fig. 23 Temperature dependence of center wavelength measured using an external heater.

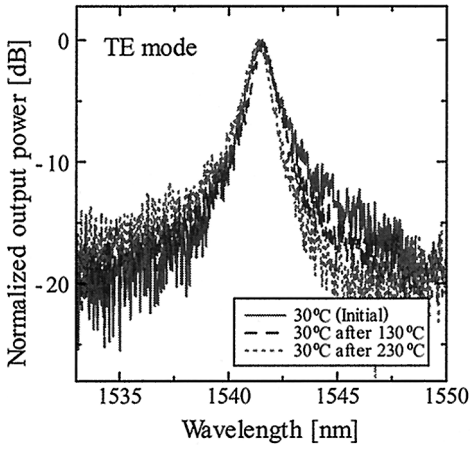

Fig. 24 Reproducibility of filter response after heat cycle.

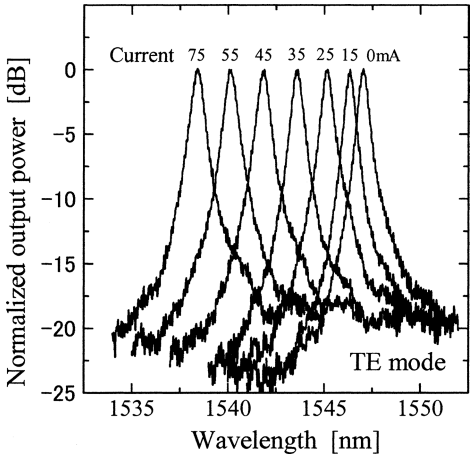

Fig. 25 Tuning of center wavelength by integrated microheater.

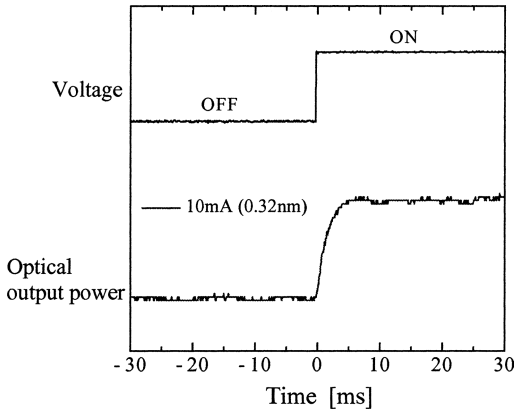

Fig. 26 Temporal response of wavelength tuning.

Table 2 Polyimides used as core material.

Type of polyimide	Index*	Birefringence	Polarization dependence of tunability*
A	1.74	0.19	-0.10nm/K
(Ref.[35])	1.55		No response
B	1.562	0.008	-0.10nm/K
(Ref.[36])	1.554		-0.07nm/K
C	1.735	0.001	-0.063nm/K
(Ref.[37])	1.736		-0.065nm/K

*Upper value: TE mode, Lower value: TM mode.

mer material used in this device is stable against heat.

The response time of the wavelength shift was measured to be 5 ms for the wavelength shift of 0.32 nm, as shown in Fig. 26. However, the response time increased for a wider tuning range. This seems to be caused by heat leakage through the electrode.

Lastly, the power consumption was evaluated to be less than 60 mW from the electric resistance of the heater (11 Ω) and the bonding wire. The reduction of power consumption will be possible by forming grooves on both sides of the microheater.

The tuning characteristics shown in Fig. 25 were obtained for only the TE mode, because the TM response was not observed due to the high birefringence of the polyimide material used in this device (n=1.74 for TE mode and n=1.55 for TM mode). Therefore, we investigated other polyimide materials, as summarized in Table 2. Polyimide A is the material used in the device shown in Fig. 25. Polyimide B has a smaller birefringence than polyimide A, and hence the TM response was observed. However, the polarization dependence of tunability remained (30%). In addition, the refractive index is not high enough to reduce the ring radius to 10 μm. Therefore, we fabricated a VCMRR using polyimide C with very small bringence as the core material and perfluorinated polymer (Cytop^{TM} by Asahi Glass Co. Ltd., n=1.333 @ λ=1.55 μm) as the cladding material.

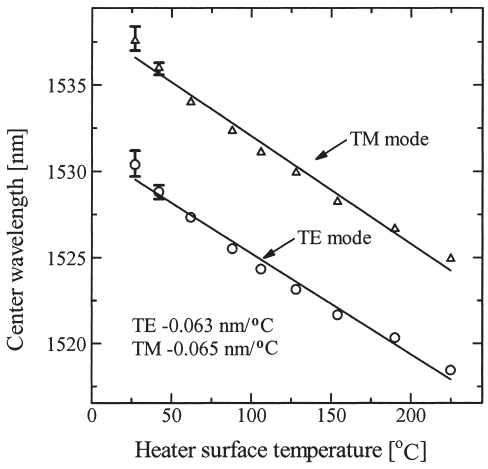

Fig. 27 Polarization dependence of tunability of TO tunable VCMRR made of polyimide C.

The ring radius was 20 μm.

The temperature dependence of the center wavelength of the polymer microring resonator was measured using an external heater. The result is shown in Fig. 27.

The center wavelength was shifted by 12.5 nm for TE and 12.9 nm for TM with the temperature increase of 200°C. From this experimental result, the temperature dependence of the center wavelength was evaluated to be −0.063 nm/°C for the TE mode and −0.065 nm/°C for TM mode. This result indicates that the polarization dependence of tunability is successfully reduced to 3% [39].

Although this device has no integrated microheater, integration with a microheater will be possible by the same fabrication process as adopted for the previous devices [37], [38]. To further reduce the polarization dependence of tunability, careful design of the cross-sectional structure will be needed to adjust the equivalent indices of TE and TM modes. With such a design, the polarization dependence of the center wavelength will also be eliminated.

Recently, a very wide tuning range of 40 nm obtained using a Vernier effect was reported [40]. In this device the center wavelength is shifted digitally by the Vernier effect between the FSR of 575 GHz and 650 GHz.

7. Buried Vacuum Cladding Structure

In Sect. 4.2, we described a vertically coupled microring resonator filter with multilevel-crossing busline waveguides. In this structure, however, there remains the problem that the radiation loss of the ring resonator increases due to the decrease of index contrast, because the ring core is covered by the cladding material.

To solve the above problem, we developed a novel fabrication process that enables the stacked dense integration of VCMRR buried by SiO_2 cladding with a vacuum side cladding, as shown in Fig. 28 [41]. Owing to vertical coupling between the busline and ring resonator and the ultrahigh index contrast of the vacuum side cladding, the radia-

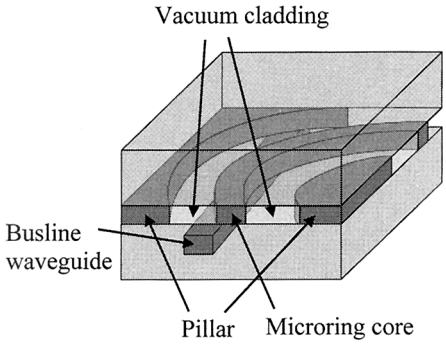

Fig. 28 Vertically coupled microring resonator with buried vacuum structure as side cladding.

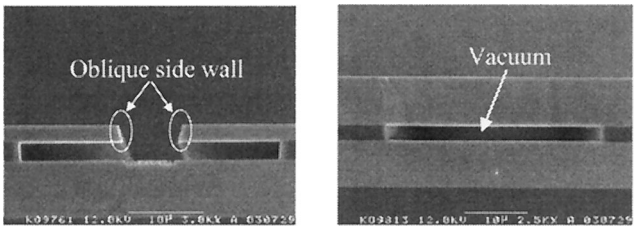

(a) Before sputtering deposition. (b) After sputtering deposition.

Fig. 29 Cross-sectional SEM view of the fabrication process of buried vacuum cladding structure.

tion loss in the ring resonator can be greatly reduced without affecting the coupling strength.

When two ridge structures are close together, a buried vacuum channel can be formed between the two ridge structures after burying them by ordinary sputtering deposition of dielectric film. Utilizing this property, we can fabricate an optical waveguide, the core of which is buried by cladding material in the vertical direction but sandwiched by vacuum cladding in the lateral direction. Thus high index contrast can be realized in the lateral direction, which is needed to achieve an ultrasmall ring radius ($< 10\,\mu$m). The vertical coupling can be achieved through the dielectric cladding layer, as shown in Fig. 28.

The fabrication process is as follows. First a planar waveguide structure with a SiN (n=2.06 @ λ=1550 nm) core and SiO_2 (n=1.452 @ λ=1550 nm) cladding is formed. Next a groove is formed through the upper SiO_2 cladding and the SiN core by photolithography and reactive ion etching (RIE). Then the SiN core layer is selectively side-etched by H_3PO_4, as shown in Fig. 29(a). In the final process, the wing of the upper SiO_2 cladding is buried by SiO_2 deposited by RF sputtering, as shown in Fig. 29(b).

Figure 30 shows the theoretical radiation losses of ring waveguides buried by SiO_2 cladding and vacuum side cladding. It is seen that the ultracompact ring radius of $< 5\,\mu$m is very difficult to obtain with the buried SiO_2 cladding structure, while it is possible to obtain with the vacuum side cladding.

Using this technique, a single-ring resonator with a $5\,\mu$m ring radius was fabricated and the filter response was

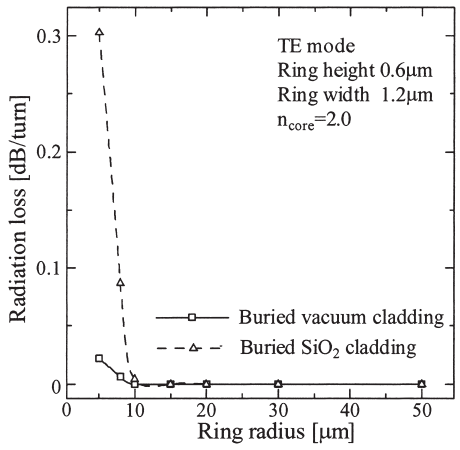

Fig. 30 Comparison of theoretical radiation loss of VCMRR with buried SiO_2 cladding and buried vacuum cladding.

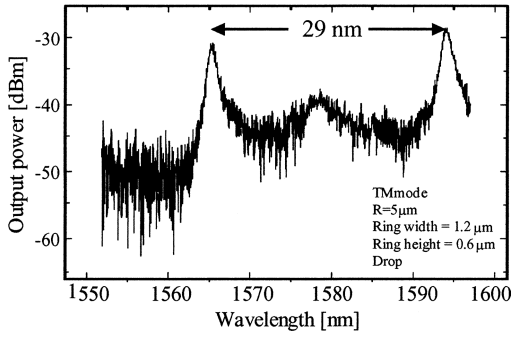

Fig. 31 Measured filter response of VCMRR with buried vacuum cladding ($R = 5\,\mu$m).

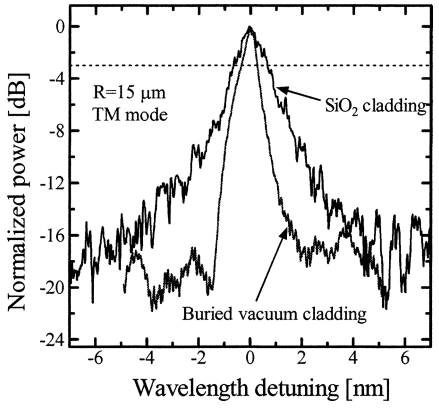

Fig. 32 Comparison of drop port responses of VCMRR with buried SiO_2 cladding and buried vacuum cladding ($R = 15\,\mu$m).

measured. The measured result of the drop port response is shown in Fig. 31. The FSR of 29 nm and the FWHM bandwidth of 1.2 nm were clearly observed.

Figures 32 and 33 show the drop port and through port responses of VCMRR fabricated by this process and those fabricated by the previous process, respectively. The structures and the index of each layer are the same for both devices, except for the existence of the vacuum cladding.

The results indicate that the loss in the ring was greatly

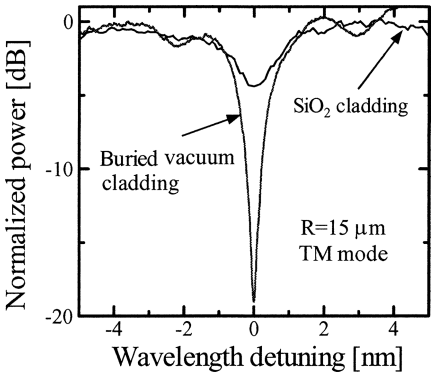

Fig. 33 Comparison of through port responses of VCMRR with buried SiO_2 cladding and buried vacuum cladding ($R = 15\,\mu$m).

reduced, because the FWHM of the device fabricated by our process (0.61 nm) is smaller than that of the device fabricated by the previous process (1.35 nm). In addition, the transmittance to the drop port is as large as 99%, because the drop depth in the through port response is about 20 dB. The loss α in the ring resonator can be evaluated from the FWHM of the drop port response and the rejection of the through port response at on-resonance [27]. The evaluated α is 0.13 dB/turn for the buried vacuum cladding structure and 1.4 dB/turn for the buried SiO_2 cladding structure. The discrepancy between the experimental and theoretical results may be attributed to scattering loss in the microring resonator.

8. Conclusion

The vertically coupled microring resonator filter can satisfy most of the optical filter requirements because of the dense integration and the layout design of elements on the crossing points of cross-grid busline waveguides. In the cascaded filter, the overall filter response is expressed by the product of responses of individual filters, and the FSR is expanded. The filter elements can also be arranged in a line to form a filter array. In series coupling, the pass band is flattened and the FSR is expanded. Parallel coupling can function as a multiport interleaver [42].

The remaining issues which must be solved to enable practical use in communication are the temperature and polarization dependences of center wavelengths. The temperature dependence has already been solved by using an athermal waveguide [43], [44] and a polarization-independent VCMRR achieved by using a birefringent polymer overlay has already been demonstrated [45]. The polarization dependence can also be eliminated by carefully designing the aspect ratio of the cross section of the microring waveguide.

Therefore, the cross-grid topology and the stacked configuration will enable a dense integration and the synthesis of many kinds of filters, and will open up the door to VLSI photonics, as shown in Fig. 34.

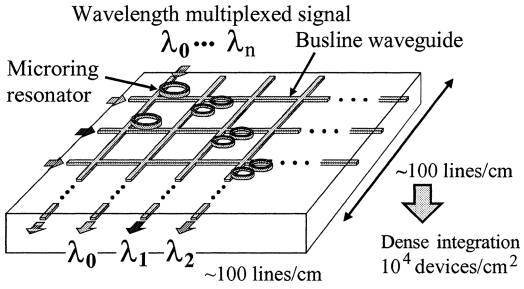

Fig. 34 VLSI photonic circuit utilizing VCMRR as the building block and the cross-grid topology of busline waveguides.

Acknowledgments

This work was supported in part by Grant-in-Aid for Scientific Research on Priority Areas No.13026210 from the Ministry of Education, Culture, Sports, Science and Technology, the Futaba Electronics Memorial Foundation, and the 21st Century COE Program in the Ministry of Education, Culture, Sports, Science and Technology.

References

[1] F. Tian, C. Harizi, H. Herrmann, V. Reimann, R. Ricken, U. Rust, W. Sohler, F. Wehrmann, and S. Westenhofer, "Polarization-independent integrated optical, acoustically tunable double-stage wavelength filter in $LiNbO_3$," IEEE/OSA J. Lightwave Technol., vol.12, no.7, pp.1192–1197, July 1994.

[2] H.S. Park, K.Y. Song, S.H. Yun, and B.Y. Kim, "All-fiber wavelength-tunable acoustooptic switches based on intermodal coupling in fibers," IEEE/OSA J. Lightwave Technol., vol.20, no.10, pp.1864–1868, Oct. 2002.

[3] K.O. Hill and G. Melts, "Fiber Bragg grating technology fundamentals and overview," IEEE/OSA J. Lightwave Technol., vol.15, no.8, pp.1263–1276, Aug. 1997.

[4] R.C. Alferness, L.L. Buhl, M.J.R. Martyak, M.D. Divino, C.H. Joyner, and A.G. Dentai, "Narrowband GaInAsP/InP waveguide grating-folded directional coupler multiplexer/demultiplexer," Electron. Lett., vol.23, no.3, pp.150–151, Feb. 1988.

[5] G.E. Kohnke, C.H. Henry, E.J. Laskowski, M.A. Cappuzo, T.A. Strasser, and A.E. White, "Silica based Mach-Zehnder add-drop filter fabricated with UV induced gratings," Electron. Lett., vol.32, no.17, pp.1579–1580, Aug. 1996.

[6] T. Amano, F. Koyama, T. Hino, M. Arai, and A. Matsutani, "Design and fabrication of GaAs-GaAlAs micromachined tunable filter with thermal strain control," IEEE/OSA J. Lightwave Technol., vol.21, no.3, pp.596–601, March 2003.

[7] B.E. Little, S.T. Chu, H.A. Haus, J. Foresi, and J.-P. Laine, "Microring resonator channel dropping filters," IEEE/OSA J. Lightwave Technol., vol.15, no.6, pp.998–1005, June 1997.

[8] S.C. Hagness, D. Rafizadeh, S.T. Ho, and A. Taflove, "FDTD microcavity simulations: Design and experimental realization of waveguide-coupled single-mode ring and whispering-gallery-mode disk resonators," IEEE/OSA J. Lightwave Technol., vol.15, no.11, pp.2154–2165, Nov. 1997.

[9] D. Rafizadeh, J.P. Zhang, S.C. Hagness, A. Taflove, K.A. Stair, S.T. Ho, and R.C. Tiverio, "Waveguide-coupled AlGaAs/GaAs microcavity ring and disk resonators with high finesse and 21.6 nm free spectral range," Opt. Lett., vol.22, no.16, pp.1244–1246, Aug. 1997.

[10] B.E. Little, J.S. Foresi, G. Steinmeyer, E.R. Thoen, S.T. Chu, H.A. Haus, E.P. Ippen, L.C. Kimerling, and W. Greene, "Ultra-compact

Si/SiO_2 microring resonator optical channel dropping filters," IEEE Photonics Technol. Lett., vol.10, no.4, pp.549–551, April 1998.
[11] C.K. Madsen and G. Lenz, "Optical all-pass filters for phase response design with applications for dispersion compensation," IEEE Photonics Technol. Lett., vol.10, no.7, pp.994–996, July 1998.
[12] C.K. Madsen, G. Lenz, A.J. Bruce, M.A. Capuzzo, L.T. Gomez, T.N. Nielsen, and I. Brener, "Multistage dispersion compensator using ring resonators," Opt. Lett., vol.24, no.22, pp.1555–1557, Nov. 1999.
[13] V. Van, T.A., Ibrahim, K. Ritter, P.P. Absil, F.G. Johnson, R. Grover, J. Goldhar, and P.-T. Ho, "All-optical nonlinear switching in GaAs-AlGaAs microring resonators," IEEE Photonics Technol. Lett., vol.14, no.1, pp.74–76, Jan. 2002.
[14] J. Azana and L.R. Chen, "Multiwavelength optical signal processing using multistage ring resonators," IEEE Photonics Technol. Lett., vol.14, no.5, pp.654–656, May 2002.
[15] B.E. Little, S.T. Chu, W. Pan, D. Ripin, T. Kaneko, Y. Kokubun, and E. Ippen, "Vertically coupled glass microring resonator channel dropping filters," IEEE Photonics Technol. Lett., vol.11, no.2, pp.215–217, Feb. 1999.
[16] S.T. Chu, B.E. Little, W. Pan, T. Kaneko, S. Sato, and Y. Kokubun, "An eight-channel add-drop filter using vertically coupled microring resonators over a cross grid," IEEE Photonics Technol. Lett., vol.11, no.6, pp.691–693, June 1999.
[17] S.T. Chu, W. Pan, S. Sato, T. Kaneko, B.E. Little, and Y. Kokubun, "Wavelength trimming of a microring resonator filter by means of a UV sensitive polymer overlay," IEEE Photonics Technol. Lett., vol.11, no.6, pp.688–690, June 1999.
[18] S.T. Chu, W. Pan, S. Suzuki, B.E. Little, S. Sato, and Y. Kokubun, "Temperature insensitive vertically coupled microring resonator Add/Drop filters by means of a polymer overlay," IEEE Photonics Technol. Lett., vol.11, no.9, pp.1138–1140, Sept. 1999.
[19] S.T. Chu, B.E. Little, W. Pan, T. Kaneko, and Y. Kokubun, "Cascaded microring resonators for crosstalk reduction and spectrum cleanup in Add-Drop filters," IEEE Photonics Technol. Lett., vol.11, no.11, pp.1423–1425, Nov. 1999.
[20] S.T. Chu, B.E. Little, W. Pan, T. Kaneko, and Y. Kokubun, "Second-order filter response from parallel coupled glass microring resonators," IEEE Photonics Technol. Lett., vol.11, no.11, pp.1426–1428, Nov. 1999.
[21] B.E. Little, S.T. Chu, W. Pan, and Y. Kokubun, "Microring Resonator Arrays for VLSI photonics," IEEE Photonics Technol. Lett., vol.12, no.3, pp.323–325, March 2000.
[22] S. Suzuki, Y. Hatakeyama, Y. Kokubun, and S.T. Chu, "Precise control of wavelength channel spacing of microring resonator Add/Drop filter array," IEEE/OSA J. Lightwave Technol., vol.20, no.4, pp.745–750, April 2002.
[23] E.A.J. Marcatili, "Bends in optical dielectric guides," Bell Syst. Tech. J., vol.48, pp.2103–2132, Sept. 1969.
[24] S. Suzuki, K. Shuto, and Y. Hibino, "Integrated optic ring resonators with two stacked layers of slica waveguides on Si," IEEE Photonics Technol. Lett., vol.4, no.11, pp.1256–1258, Nov. 1992.
[25] M.K. Chin, C. Youtsey, W. Zhao, T. Pierson, Z. Ren, S.L. Wu, L. Wang, Y.G. Zhao, and S.T. Ho, "GaAs microcavity channel-dropping filter based on a race-track resonator," IEEE Photonics Technol. Lett., vol.11, no.12, pp.1620–1622, Dec. 1999.
[26] Y. Hatakeyama, T. Hanai, S. Suzuki, and Y. Kokubun, "Loss-less multilevel crossing of busline waveguide in vertically coupled microring resonator filter," IEEE Photonics Technol. Lett., vol.16, no.2, pp.473–475, Feb. 2004.
[27] T. Ito and Y. Kokubun, "Non-destructive measurement of loss and coupling efficiency in microring resonator filters from filter responses," Jpn. J. Appl. Phys., vol.43, no.3, pp.1002–1005, March 2004.
[28] T. Kato, S. Suzuki, Y. Kokubun, and S.T. Chu, "Coupling loss reduction of vertically coupled microring resonator filter by spot size matched busline waveguides," Appl. Opt., vol.41, no.21, pp.4394–4399, July 2002.
[29] J.V. Hryniewicz, P.P. Absil, B.E. Little, R.A. Wilson, and P.-T. Ho, "Higher order filter response in coupled microring resonators," IEEE Photonics Technol. Lett., vol.12, no.3, pp.320–322, March 2000.
[30] Y. Yanagase, S. Suzuki, Y. Kokubun, and S.T. Chu, "Vertical triple series-coupled microring resonator filter for pass band flattening and expansion of free spectral range," Jpn. J. Appl. Phys., vol.41, no.2A, pp.L141–L143, Feb. 2002.
[31] Y. Yanagase, S. Suzuki, Y. Kokubun, and S.T. Chu, "Box-like filter response and expansion of FSR by vertically triple coupled microring resonator filter," IEEE/OSA J. Lightwave Technol., vol.20, no.8, pp.1525–1529, Aug. 2002.
[32] P.P. Absil, S.T. Chu, D. Gill, J.V. Heryniewicz, F. Johnson, O. King, B.E. Little, F. Seiferth, and V. Van, "Very high order integrated optical filters," Optical Fiber Conference (OFC2004), Los Angeles, TuL3, Feb. 2004.
[33] Y. Kokubun, H. Haeiwa, and H. Tanaka, "Precise center wavelength trimming of vertically coupled microring resonator filter by direct UV irradiation to ring core," IEEE/LEOS Annual Meeting, Glasgow, ThN3, Nov. 2002.
[34] H. Haeiwa, T. Naganawa, and Y. Kokubun, "Wide range center wavelength trimming of vertically coupled microring resonator filter by direct UV irradiation to SiN ring core," IEEE Photonics Technol. Lett., vol.16, no.1, pp.135–137, Jan. 2004.
[35] T. Naganawa, H. Haeiwa, and Y. Kokubun, "UV induced refractive index change of SiN film and its application to center wavelangth trimming of vertically coupled microring resonator filter," Jpn. J. Appl. Phys., vol.43, no.8B, pp.5780–5784, Aug. 2004.
[36] S. Suzuki, K. Oda, and Y. Hibino, "Integrated-optic double-ring resonators with a wide free spectral range of 100 GHz," IEEE/OSA J. Lightwave Technol., vol.13, no.8, pp.1766–1771, Aug. 1995.
[37] Y. Yanagase, S. Yamagata, and Y. Kokubun, "Wavelength tunable polymer microring resonator filter with 9.4 nm tuning range," Electron. Lett., vol.39, no.12, pp.922–924, June 2003.
[38] S. Yamagata, Y. Yanagase, and Y. Kokubun, "Wide range tunable microring resonator filter by thermo-optic effect in polymer waveguide," Jpn. J. Appl. Phys., vol.43, no.8B, pp.5766–5770, Aug. 2004.
[39] G. Sekiguchi, S. Yamagata, and Y. Kokubun, "Polarization independent tuning of widely tunable vertically coupled microring resonator by thermo-optic effect," 9th OptoElectronics and Communications Conference/3rd International Conference on Optical Internet (OECC/ COIN2004), Yokohama, 13F2-4, July 2004.
[40] S.T. Chu, B.E. Little, V. Van, J.V. Heryniewicz, P.P. Absil, F.G. Johnson, D. Gill, O. King, F. Seiferth, M. Trakalo, and J. Shanton, "Compact full C-band tunable filters for 50 GHz channel spacing based on high order micro-ring resonators," Optical Fiber Conference (OFC2004), Los Angeles, PDP9, Feb. 2004.
[41] M. Ogata, Y. Yoda, S. Suzuki, and Y. Kokubun, "Ultra-compact vertically coupled microring resonator with buried vacuum cladding structure," IEEE Photonics Technol. Lett., vol.17, no.1, pp.103–105, Jan. 2005.
[42] T. Ito and Y. Kokubun, "Fabrication of interleaver by parallel coupled ring resonator," 9th OptoElectronics and Communications Conference/3rd International Conference on Optical Internet (OECC/COIN2004), Yokohama, PD2-6, July 2004.
[43] S.T. Chu, W. Pan, S. Suzuki, B.E. Little, S. Sato, and Y. Kokubun, "Temperature insensitive vertically coupled microring resonator Add/Drop filters by means of a polymer overlay," IEEE Photonics Technol. Lett., vol.11, no.9, pp.1138–1140, Sept. 1999.
[44] Y. Kokubun, S. Yoneda, and S. Matsuura, "Athermal narrow-band optical filter at 1.55 μm wavelength by silica-based athermal waveguide," IEICE Trans. Electron., vol.E-81C, no.8, pp.1187–1194, Aug. 1998.
[45] Y. Kokubun, S. Kubota, and S.T. Chu, "Polarisation independent vertically coupled microring resonator filter," Electron. Lett., vol.37, no.2, pp.90–92, Feb. 2001.

Yasuo Kokubun received his B.E. degree from Yokohama National University, Yokohama, Japan, in 1975 and M.E. and Dr. Eng. degrees from Tokyo Institute of Technology, Tokyo, Japan, in 1977 and 1980, respectively. After he worked for the Research Laboratory of Precision Machinery and Electronics, Tokyo Institute of Technology, as a research associate from 1980 to 1983, he joined the Yokohama National University as an associate professor in 1983, and is now a professor in the Department of Electrical and Computer Engineering. His current research is in integrated photonics, particularly waveguide-type functional devices and three-dimensional integrated photonics. From 1984 to 1985 he was with AT&T Bell Laboratories, Holmdel, NJ, as a visiting reseacher and was engaged in the study of a novel waveguide on a semiconductor substrate (ARROW) for integrated optics. From 1996 to 1999, he served as the project leader of the "Three-dimensional microphotonics" project at the Kanagawa Academy of Science and Technology." Professor Kokubun is a member of the Institute of Electrical and Electronics Engineers, the Japan Society of Applied Physics, and the Optical Society of America.